Stability of *p*-orbital Bose-Einstein condensates in optical checkerboard and square lattices

Yong Xu (徐勇),[1,2] Zhu Chen (陈竹),[3] Hongwei Xiong (熊宏伟),[4,5] W. Vincent Liu (刘文胜),[6] and Biao Wu (吴飙)[2,*]

[1]*Institute of Physics, Chinese Academy of Sciences, Beijing 100190, China*

[2]*International Center for Quantum Materials, Peking University, Beijing 100871, China*

[3]*Institute for Advanced Study, Tsinghua University, Beijing 100084, China*

[4]*State Key Laboratory of Magnetic Resonance and Atomic and Molecular Physics, Wuhan Institute of Physics and Mathematics, Chinese Academy of Sciences, Wuhan 430071, China*

[5]*Department of Applied Physics, Zhejiang University of Technology, Hangzhou 310023, China*

[6]*Department of Physics and Astronomy, University of Pittsburgh, Pittsburgh, Pennsylvania 15260, USA*

(Received 3 December 2012; published 29 January 2013)

We investigate *p*-orbital Bose-Einstein condensates in both the square and checkerboard lattice by numerically solving the Gross-Pitaevskii equation. The periodic potential for the latter lattice is taken exactly from the recent experiment [Nature Phys. **7**, 147 (2011)]. It is confirmed that the staggered orbital-current state is the lowest-energy state in the *p* band. Our numerical calculation further reveals that for both lattices the staggered *p*-orbital state suffers Landau instability but the situation is remarkably different for dynamical instability. A dynamically stable parameter region is found for the checkerboard lattice, but not for the square.

DOI: 10.1103/PhysRevA.87.013635 PACS number(s): 03.75.Kk, 03.75.Lm, 37.10.Jk, 05.30.Jp

I. INTRODUCTION

Orbital physics is important in solid-state material due to its key role in understanding many interesting phenomena including metal-insulator transition, unconventional superconductivity, and colossal magnetoresistance [1]. However, to fully understand the role of orbital degree of freedom in real solid materials is challenging because of their complex nature. A quantum degenerate gas in the optical lattice [2,3], which is disorder free and highly tunable, is an ideal platform to explore high orbital physics as the orbital degree of freedom in such an ultracold gas is separate from spin and charge freedom automatically. Moreover, a system of neutral bosons loaded into an optical lattice at low enough temperature has no counterpart in real quantum materials. Bosonic atoms can condensate into non-ground state, opening the possibility to explore physics that previously might have seemed academic or impossible, e.g., the time-reversal symmetry breaking superfluidity in the nodal *p* band [4–6].

Several experimental methods have been developed to populate the *p* and higher orbital bands in optical lattices [7–16]. Pioneering experiments have been carried out by accelerating the lattice [7], dynamically deforming the double-well potentials as a single-site manipulation [8–11], and exciting atoms into the higher vibrational state along a controlled lattice direction through stimulated Raman transitions [12]. The recent implementation of orbital degrees of freedom in checkerboard [13–15] and hexagonal [16] optical lattices truly opens an era of exploring orbital phases of quantum matter that have no prior analogues in solid-state materials. For example, the experiments of Ölschlärger *et al.* [13–15] show that bosonic atoms are loaded and kept in the excited *p*-orbital bands for nearly as long as the ultracold gases can be, thus effectively possessing infinite long lifetime in the scale of tunneling. In the experiment, atoms are transferred from the *s*-orbital band to the *p*-orbital band through the changing of the double-well relative depth, the time of flight images have illustrated the macroscopic occupation in the *p*-orbital real state and complex state. The same group also reported the observation of the exotic *d*- and *f*-band superfluid phases [14,15]. Dynamically, fermionic and bosonic atoms are made across from lower to high orbital bands in optical honeycomb [17] and checkerboard [15] lattices, respectively.

Although the experiments are done with continuous optical potential of periodic oscillation, most of the past theoretical work employed the standard tight-binding method and approximated the system to a lattice model, where the atoms are strictly constrained to the *p* orbital. Many interesting results have been worked out, such as the staggered state as the ground state in the *p*-orbital band [5], superfluid transition to Mott phase [4,18,19], supersolid quantum phase [20], and quantum strip ordering in triangular lattices [21] (for other interesting studies and a brief perspective, see, for example, Ref. [22]). In this work, we use the continuous model where little theoretical work has been done besides a variational computation of the lowest energy in the *p*-orbital band [23]. The continuous model provides a better and complete description of the system as it can capture the decay to the *s* band that happens in real experiments and applies beyond tight-binding approximation. We focus on the stability of the *p*-orbital state, which is crucial to understand the *p*-band superfluidity. To understand the superfluidity in the *s* band, stability of the Bloch states in the *s* band has been analyzed theoretically for different lattices—one-dimensional lattices [24], two-dimensional square lattices [25], and two-dimensional double-well lattices [26]. It was also investigated experimentally for a one-dimensional lattice [27]. However, for the *p*-orbital system, to the best of our knowledge, only one paper [28] discussed the dynamical instability and it is limited to the one-dimensional case.

In this paper, with the Gross-Pitaevskii (GP) equation, we calculate exactly the *p*-orbital band ground state for both the two-dimensional (2D) square optical lattice and the checkerboard lattice used in the experiment [13]. We confirm that the lowest-energy state in the *p* band is the staggered state found in Ref. [5]. The Landau instability and dynamical

*wubiao@pku.edu.cn

instability of this state are investigated. For the lattice model approach, such a study of stability is not accurate because the s band is always removed from the Hamiltonian to make the condensate impossible to decay. Our calculation shows that, for both periodic potentials, the staggered state always has Landau instability as the state is a local saddle point that can decay into the s band. For the dynamical stability, these two 2D lattices are very different: our numerical search does not find any parameter region for the square lattice, where the staggered state is dynamically stable; in contrast, there exists a parameter region for the checkerboard potential where the staggered state is dynamically stable. This is consistent with the intuitive understanding that the checkerboard potential offers better stability [29]. That is, on general ground, the checkerboard potential may be viewed as a particular configuration of the simple double-well lattice potential, and the energy gap between the lowest s and the first excited p orbital bands is much smaller than that between the p and the higher excited bands. Consequently, the first-order decay of atoms in the p band due to scattering for the checkerboard lattice is suppressed by energy conservation according to Fermi golden rule, in contrast with the decay for the square lattice of single wells where band spacings are approximately equal in the tight-binding (i.e., the simple harmonic oscillator) limit.

The paper is organized in the following way. In Sec. II, the general theoretical framework of our calculation is given. In Secs. III and IV, the results for both the square lattice and the checkerboard lattice are presented, respectively. Finally, conclusions are drawn in Sec. V.

II. GENERAL THEORETICAL FRAMEWORK

We consider the Bose-Einstein condensate of bosons in a 2D optical potential with periodicity characterized by two lattice vectors to be defined below. To compare with realistic three-dimensional experimental systems, our model applies to the experiments where a strong trap is applied along the third direction. We thus neglect the third dimension, which only contributes to the effective interaction parameter. The 2D GP equation is

$$i\hbar\partial_t\psi(\mathbf{r}) = \left[-\frac{\hbar^2}{2m}\nabla^2 + V(\mathbf{r}) + g|\psi|^2\right]\psi(\mathbf{r}), \tag{1}$$

where $V(\mathbf{r}+\mathbf{a}_1) = V(\mathbf{r}+\mathbf{a}_2) = V(\mathbf{r})$ with $\mathbf{a}_1$ and $\mathbf{a}_2$ the lattice vectors; m is the atomic mass, and g is the interaction parameter. $\psi(\mathbf{r})$ is normalized as $\frac{1}{\Omega}\int_\Omega |\psi(\mathbf{r})|^2 d\mathbf{r} = 1$ where the subscript Ω indicates an integral over the unit cell with an area $\Omega = |\mathbf{a}_1||\mathbf{a}_2|$.

We are interested in the lowest-energy state in the p-orbital band. This type of state must be stationary and satisfy the time-independent GP equation

$$\left[-\frac{\hbar^2}{2m}\nabla^2 + V(\mathbf{r}) + g|\psi|^2\right]\psi(\mathbf{r}) = \mu\psi(\mathbf{r}), \tag{2}$$

where μ is the chemical potential. The extended solution to the above nonlinear periodic equation has the form $\psi(\mathbf{r}) = e^{i\mathbf{k}\cdot\mathbf{r}} f(\mathbf{r})$. For the usual Bloch states, f is a period function with the same period as that of the optical lattice, $f(\mathbf{r}+\mathbf{a}_1) = f(\mathbf{r})$ and $f(\mathbf{r}+\mathbf{a}_2) = f(\mathbf{r})$. Besides Bloch states, there are other solutions such as the period-doubled solutions [25,30], where f satisfies $f(\mathbf{r}+2\mathbf{a}_1) = f(\mathbf{r})$ and $f(\mathbf{r}+2\mathbf{a}_2) = f(\mathbf{r})$. For the s band, the usual Bloch states always have lower energy than that of period-doubled states. But for the p-orbital band, previous studies [5,23] have shown that the period-doubled solution has lower energy than the corresponding Bloch state due to the extra π phase in p-orbital tunneling.

For the two types of lattices considered in this work, the following two Bloch states are degenerate and have the lowest energy among all the Bloch states,

$$P_x = \sum_{\mathbf{G}} u_{\mathbf{G}} e^{i(\mathbf{k}_1+\mathbf{G})\cdot\mathbf{r}}, \tag{3}$$

and

$$P_y = \sum_{\mathbf{G}} v_{\mathbf{G}} e^{i(\mathbf{k}_2+\mathbf{G})\cdot\mathbf{r}}, \tag{4}$$

where $\mathbf{G} = m\mathbf{b}_1 + n\mathbf{b}_2$, $\mathbf{b}_1$, and $\mathbf{b}_2$ are reciprocal lattice vectors, and $\mathbf{k}_1 = \mathbf{b}_1/2$ and $\mathbf{k}_2 = \mathbf{b}_2/2$. Substituting these two equations into Eq. (2) leads to a series of nonlinear equations of either u or v. We use the subroutine fsolve of MATLAB to solve these equations.

There are other types of solutions, which can be symbolically expressed as either

$$P_{x\pm y} = \frac{1}{\sqrt{2}}(P_x \pm P_y), \tag{5}$$

or

$$P_{x\pm iy} = \frac{1}{\sqrt{2}}(P_x \pm iP_y). \tag{6}$$

These solutions are period-doubled states and therefore non-Bloch. Without interaction, these non-Bloch states would have the same energy as the Bloch states P_x and P_y. With interaction, these states may break the degeneracy, splitting into either lower or higher energy. To find these non-Bloch states, one can similarly substitute Eqs. (5) and (6) into Eq. (2) and find the coefficients u and v numerically. The coefficients u and v found here are in general different from the ones found by substituting Eqs. (3) and (4) into Eq. (2). This is the essential technical difference from the work in Ref. [23]. Due to the time-reversal symmetry, it is sufficient to consider only P_{x+y} and P_{x+iy}.

We are interested in the stability of these p-orbital states. We know that the lowest-energy state in the s band is always stable because it is the lowest-energy state of the system. It is imperative to know whether the lowest-energy p-orbital state is stable or not. In fact, this was already the concern at the beginning of studying the p-orbital states in cold-atom systems [5,6] as the decay to the s band seems almost inevitable. However, it is possible that interaction may be able to stabilize a certain p-orbital state and make it a metastable state. The primary purpose of this work is to answer whether such a possibility exists. As will be shown later, the state P_{x+iy} always has the lowest energy among all examined p-orbital states. Consequently, we will focus on the stability of this state.

To examine the stabilities of a state, one can follow the well-known procedure [24] and obtain the Bogoliubov equation in momentum $\mathbf{q}$ space

$$\epsilon_{\mathbf{q}}\begin{pmatrix} u_{\mathbf{q}} \\ v_{\mathbf{q}} \end{pmatrix} = \sigma_z M \begin{pmatrix} u_{\mathbf{q}} \\ v_{\mathbf{q}} \end{pmatrix}, \tag{7}$$

where σ_z is the Pauli matrix. For the state P_{x+iy}, we have

$$M = \begin{pmatrix} \mathcal{L}(\mathbf{q}) & gP_{x+iy}^2 \\ gP_{x+iy}^{*2} & \mathcal{L}(\mathbf{q}) \end{pmatrix}, \tag{8}$$

with

$$\mathcal{L}(\mathbf{q}) = -\frac{\hbar^2}{2m}[(\partial_x + iq_x)^2 + (\partial_y + iq_y)^2] + V(\mathbf{r}) - \mu_{xy} + 2g|P_{x+iy}|^2. \tag{9}$$

Since P_{x+iy} is period doubled, we have $u_{\mathbf{q}}(\mathbf{r}+2\mathbf{a}_1) = u_{\mathbf{q}}(\mathbf{r}+2\mathbf{a}_2) = u_{\mathbf{q}}(\mathbf{r})$ and $v_{\mathbf{q}}(\mathbf{r}+2\mathbf{a}_1) = v_{\mathbf{q}}(\mathbf{r}+2\mathbf{a}_2) = v_{\mathbf{q}}(\mathbf{r})$. To numerically diagonalize the matrix $\sigma_z M$, we expand u and v in Fourier series as $u_{\mathbf{q}}(\mathbf{r}) = \sum_{\mathbf{G}} u_{\mathbf{G}} e^{i\mathbf{G}\cdot\mathbf{r}/2}$ and $v_{\mathbf{q}}(\mathbf{r}) = \sum_{\mathbf{G}} v_{\mathbf{G}} e^{i\mathbf{G}\cdot\mathbf{r}/2}$. The diagonalization of $\sigma_z M$ for the phonon modes yields the Bogoliubov excitation of the state P_{x+iy}. This state has Landau instability if part of its Bogoliubov excitations is negative; it has dynamical instability if part of its Bogoliubov excitations is imaginary [25].

III. SQUARE LATTICE

The square lattice can be formed by simply overlapping two counterpropagating laser beams. Mathematically, it is described by $V(x,y) = V_0[\cos(x) + \cos(y)]$. For this lattice, it is convenient to use the following time-independent GP equation

$$\left[-\frac{1}{2}\left(\partial_x^2 + \partial_y^2\right) + V(x,y) + c|\psi|^2\right]\psi(x,y) = \mu\psi(x,y). \tag{10}$$

The above equation has been made dimensionless by scaling energy with $8E_r$ and length with $1/2k_L$. In this section, x and y are dimensionless. E_r is the recoil energy and $k_L = 2\pi/\lambda$ is the wave vector of the laser beam. The interaction constant is $c = mng/\hbar^2$ with m being the atom mass, n the BEC density (the average particle number per site), and $g = 2\sqrt{2\pi}\hbar^2 a_s/(\sigma m)$, where a_s is the s-wave scattering length and σ is the characteristic length of the harmonic trap along the z direction.

Following the procedure described in the above section, we have numerically computed three states P_x, P_{x+y}, and P_{x+iy}. Fig. 1 illustrates how the energies and chemical potentials change with the interaction constant c for these three states. It is clear from the figure that state P_{x+iy} always has the lowest

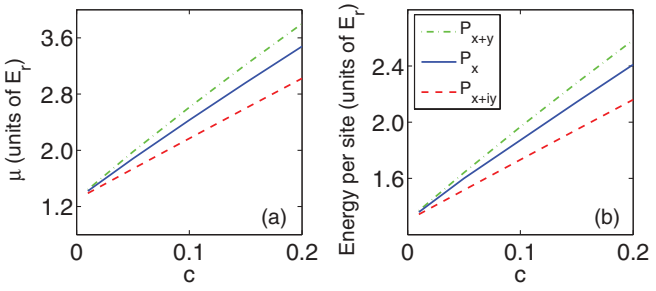

FIG. 1. (Color online) (Square lattice) Chemical potential (left) and energy per lattice site (right) for the P_x state (blue solid line), P_{x+iy} state (red dashed one) and P_{x+y} (green dashed dot line) in the square lattice. $V_0 = 0.8E_r$.

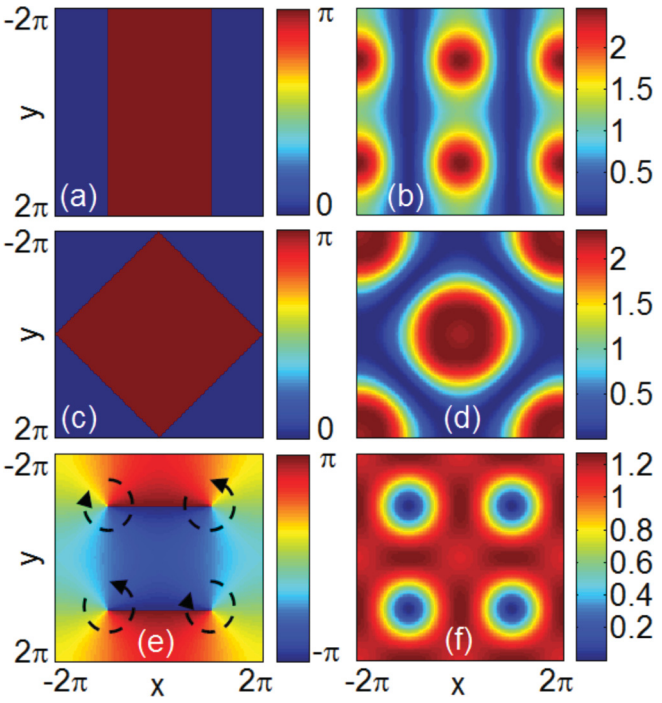

FIG. 2. (Color online) (Square lattice) Phase and density profile for state P_x (a), (b), state P_{x+y} (c), (d), and state P_{x+iy} (e), (f), respectively, for the square lattice. Arrows in (e) indicate the vortex rotating directions. For phase in (a) and (c), the dark blue is 0, the brown is π. x and y have units of $1/2k_L$. $V_0 = 0.8E_r$ and $c = 0.01$.

energy and the energy gap to the other states increases with c. This confirms the earlier results obtained with lattice model [5] and variational method [23]. It is also shown in Fig. 1 that state P_{x+y} always has the highest energy among the three.

The phase and density profiles of these three states are shown in Fig. 2. These three states not only differ in phase but also in density. Since the wave functions for both states P_x and P_{x+y} are real, their phase can only be either 0 or π. Specifically, the state P_x has a stripe phase structure while the state P_{x+y} has a square-shaped one. The wave function of the state P_{x+iy} is complex and breaks time-reversal symmetry. Consequently, this state has much richer phase structure, which is evidently shown by the staggered orbital currents in Fig. 2(e). This feature of staggered orbital currents is the most prominent predication in Ref. [5].

As the state P_{x+iy} has the lowest energy among the p-orbital states, we focus on the stability of this state. It is examined through its Bogoliubov excitations by diagonalizing the matrix $\sigma_z M$. Our computation finds that the Bogoliubov excitations always have a negative part, indicating that the P_{x+iy} has Landau instability and is not a metastable state. The situation is more delicate for dynamical stability. Figure 3 shows the phase diagram of dynamical instability, where the stars mark out the region of the (momentum) $\mathbf{q}$ space where the Bogoliubov excitations are imaginary. It is clear from the figure that the stable region of the $\mathbf{q}$ space increases as the interaction c decreases. It is reasonable to expect that the whole region be stable when c is small enough. However, within our numerical capability, we are not able to identify the values of c and V_0 for which the state P_{x+iy} is free of dynamical instability. As

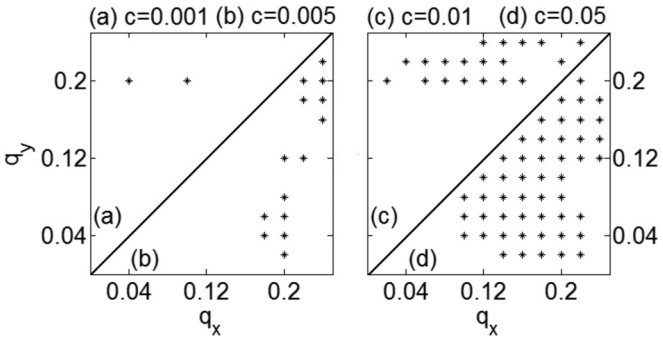

FIG. 3. (Square lattice) Dynamical stability diagram of state P_{x+iy} for the square lattice at $V_0 = 0.8E_r$. The region of dynamical instability is marked by stars. q_x and q_y are in unites of $2k_L$ with a step length 0.02. Since the diagram is symmetric with respect to q_x and q_y, we only draw the upper triangle for (a) and (c) and the lower one for (b) and (d). The upper limit for q_x and q_y is 0.25 is due to that P_{x+iy} is a period-doubled state.

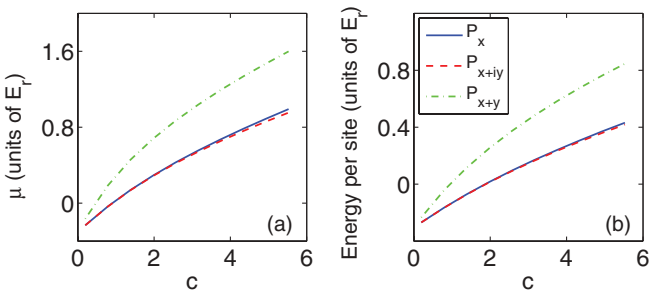

FIG. 4. (Color online) (Checkerboard lattice) Chemical potential (left) and energy per lattice well (right) for the P_x state (blue solid line), P_{x+iy} state (red dashed one), and P_{x+y} (green dashed dot one) in the checkerboard potential. $V_0 = 6.2E_r$.

shown in Figs. 3(a) and 3(b), even for very small c, there are some regions where the excitations are imaginary. This means that state P_{x+iy} is dynamically stable only for extremely small values of c. We have attempted to calculate the critical c for the typical experimental V_0 [2] and found that they are of the order of 10^{-4}. However, despite of intensive efforts, our numerical method is in capable of pinning down the exact value of these critical c as indicated by the irregular black line in the inset of Fig. 7, where the parameter region of dynamical instability for the square lattice is marked out. These results imply that it is almost impossible to use the square lattice to study p-orbital BEC states experimentally as dynamical instability can destroy a BEC in tens of milliseconds [27].

IV. CHECKERBOARD POTENTIAL

The optical lattice used in the experiment [13] is a checkerboard potential described by

$$V(x,y) = -\frac{V_0}{4}|\eta\{[\mathbf{e}_z\cos(\alpha)+\mathbf{e}_y\sin(\alpha)]e^{ik_Lx}+\epsilon\mathbf{e}_z e^{-ik_Lx}\} + e^{i\theta}\mathbf{e}_z(e^{ik_Ly}+\epsilon\mathbf{e}^{-ik_Ly})|^2, \quad (11)$$

where $\mathbf{e}_y$ and $\mathbf{e}_z$ are unit vectors in each direction. Here x and y are the space coordinates, k_L is the laser wave vector, α is the polarization angle to the z direction, ϵ is the reflection loss, η describes the small power difference between two interferometers, θ is the phase difference between the beams propagating in the x and y directions, and V_0 is determined by the laser power. The angle α can be used to adjust the degree of anisotropy: when $\alpha = \pi/5$, the energy minimum points of the two p-orbital Bloch bands are degenerate. The phase difference θ controls the relative depth of a double well. In the experiment, bosonic atoms are loaded to the p-orbital band by adjusting θ, $\eta \approx 0.95$, $\epsilon \approx 0.81$, and $V_0 = 6.2E_r$ with the recoil energy $E_r = \hbar^2k_L^2/2m$.

To have a dimensionless time-independent GP equation as in Eq. (10), we scale energy with $4E_r$ and length with $1/\sqrt{2}k_L$. In the dimensionless expression, the lattice vectors of the potential are $\mathbf{a}_1 = \sqrt{2}\pi(\mathbf{e}_x+\mathbf{e}_y)$, $\mathbf{a}_2 = \sqrt{2}\pi(-\mathbf{e}_x+\mathbf{e}_y)$ and reciprocal vectors are $\mathbf{b}_1 = (\mathbf{e}_x+\mathbf{e}_y)/\sqrt{2}$ and $\mathbf{b}_2 = (-\mathbf{e}_x+\mathbf{e}_y)/\sqrt{2}$. The quasimomentum and coordinate vector are, $\mathbf{k} = k_x\mathbf{b}_1 + k_y\mathbf{b}_2$ and $\mathbf{r} = (x\mathbf{a}_1 + y\mathbf{a}_2)/2\pi$, respectively.

We have done the same set of numerical computation for the three states P_x, P_{x+y}, and P_{x+iy} in the checkerboard lattice as in the square lattice. Figure 4 shows their energies and chemical potentials as a function of the interaction constant c. Similar to the square lattice, the state P_{x+iy} in the checkerboard lattice is found to have the lowest energy too. There is however an evident difference, i.e., for the checkerboard, the states P_{x+iy} and P_x are very close in energy while state P_{x+y} has much higher energy. This feature suggests that the state observed in the experiment [13] is probably not P_{x+y}.

The phase and density profiles of these three states are illustrated in Fig. 5. The phase profiles show a structure similar to that for the square lattice, such that P_x has the wavelike stripe phase structure, P_{x+y} has the square phase structure and P_{x+iy} has the staggered orbital currents structure [5]. This result supports the conclusion that one may use the square lattice as a simplified theoretical model to understand much of the unconventional properties of the p-orbital condensates as observed in the more complex, experimentally realized checkerboard lattice. In terms of dynamical instability, the two lattice configurations are however qualitatively different, to be elaborated below. The density profiles do not show clear difference between state P_x and P_{x+iy} and the reason is that the probability density in the deeper well where the vortex appears is very small.

For stability, we focus on that of state P_{x+iy} just as in the square lattice. We investigate it also through Bogoliubov excitations by diagonalizing the matrix $\sigma_z M$. Similar to the square lattice, our calculation shows that the Bogoliubov excitations in the checkerboard always have negative part, indicating that state P_{x+iy} in the experiment also has Landau instability. For dynamical stability, the unstable region in the $\mathbf{q}$ space increases with c as shown in Fig. 6. However, there is a crucial difference from the case of square lattice: there exists a critical value of c, below which there is no dynamical instability as indicated by the blank panel in Fig. 6(a). We are able to mark out a region in the space spanned by the system parameters c and V_0/E_r, where the P_{x+iy} state is free of dynamical instability (shown in the phase diagram Fig. 7). Due to the uncertainty of the BEC density, we have marked the experimental parameter range [13] with a solid line. This shows that it is likely that the P_{x+iy} for the experimental setup is

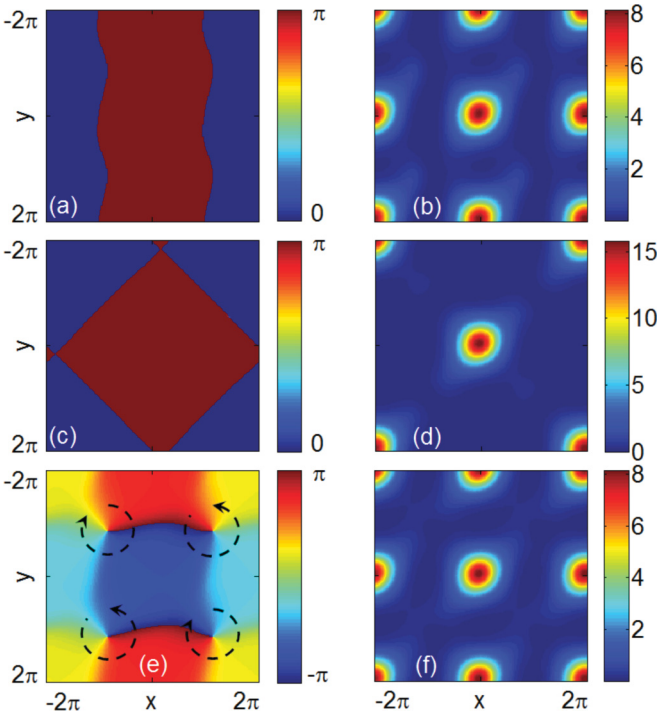

FIG. 5. (Color online) (Checkerboard lattice) Phase and density profile for state P_x (a), (b), state P_{x+y} (c), (d) and state P_{x+iy} (e), (f), respectively, in the checkerboard potential. Arrows in (e) indicate vortex rotating directions. In (a) and (c), the dark blue is for phase of 0 and the brown for phase of π. x, and y have units of $1/\sqrt{2}k_L$. $V_0 = 6.2E_r$, $c = 0.2$.

dynamically stable. Since the time scale for Landau instability is of the order of 500 ms [27], which is much longer than that of the experiment [13], it is reasonable that Landau instability does not have much effect.

In order to make sure that our calculation is correct, we simulate the real system of Eq. (1) with the split-operator method.

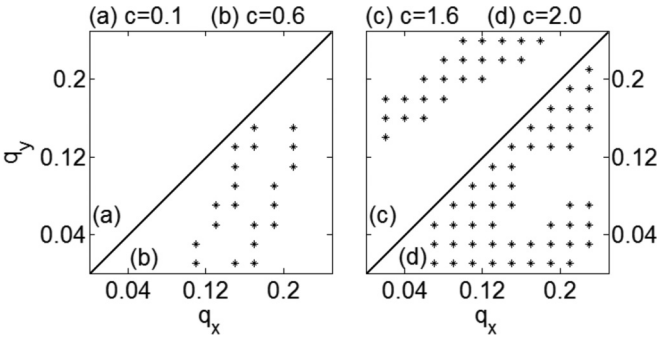

FIG. 6. (Checkerboard lattice) Dynamical stability diagram of the state P_{x+iy} of the checkerboard potential. The region of dynamical instability is marked by stars. The blank panel in (a) indicates that the system is free of dynamical instability for $c = 0.1$, to be contracted with that for the square lattice in Fig. 3. q_x and q_y are in units of $\sqrt{2}k_L$ with a step length 0.02. $V_0 = 6.2E_r$. Since the diagram is symmetric with respect to q_x and q_y, we only draw the upper triangle for (a) and (c) and the lower one for (b) and (d). The upper limit for q_x and q_y is 0.25 is due to that P_{x+iy} is a period-doubled state.

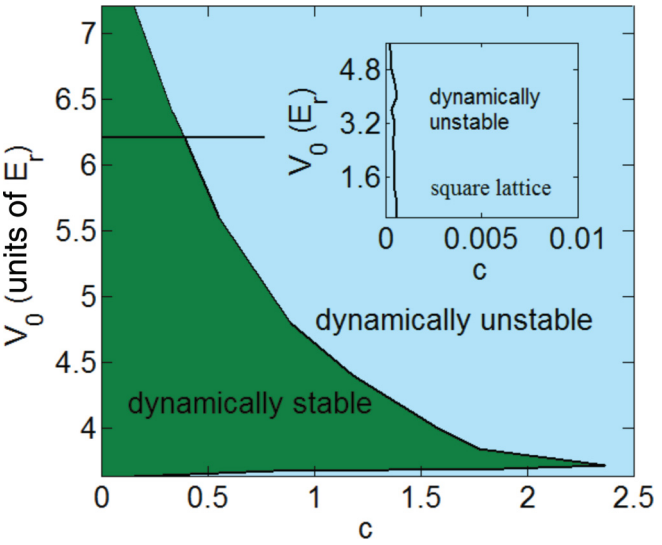

FIG. 7. (Color online) (Checkerboard lattice) Stable and unstable region in the system parameter space for state P_{x+iy} in the checkerboard potential. The black line indicates the parameter range used in the experiment [13] where $V_0 = 6.2E_r$. The inset shows the stability regions for the square lattice. The irregularity of the solid line in the inset is caused by the inability of our numerical method to compute precisely the critical value of c below which the system is dynamically stable.

We evolve numerically a BEC in the P_{x+iy} state with a small perturbation $\delta\psi$ (10%). When $c = 0.2$, the simulation shows that the state is stable. When $c = 3.0$ and $c = 7.9$, the simulation shows that the state is destroyed after $t = 17.5$ ms and $t = 2.5$ ms, respectively. All results in the three simulations are consistent with our Bogoliubov excitation calculation.

To map out the phase diagram of dynamical instability in Fig. 7 experimentally, one may need to use the Feshbach resonance to tune the interaction strength. When the Feshbach resonance is not available, one can still observe the effect of dynamical instability by turning up the laser power to drive the system into dynamically unstable regime. The effects of dynamical instability should be similar to what was observed in Ref. [27].

V. CONCLUSION

In conclusion, we have examined a cold gas of interacting bosonic atoms loaded in two optical lattice geometries, namely, the square and the checkerboard lattices, for which unconventional p-orbital Bose-Einstein condensates have been under active investigation in recent years, both theoretically and experimentally. The usual theoretical approach used in the past is to assume the standard tight-binding approximation and conveniently reduce the system to a Hubbard-like lattice model of one single orbital band of interest, i.e., the p band. The present approach is however different. Here, the model system is solved numerically with the GP equation of microscopic two-body interaction by treating the optical lattice exactly as a continuous, periodic potential, in which both the ground-state s band and all the higher orbital bands are included. The approach thus is capable of providing a complete analysis

for the Landau and dynamical instabilities of a p-orbital BEC. Such a complete analysis for instability was not considered before, to the best of our knowledge. We find that the staggered state P_{x+iy} indeed has the lowest energy in the p band. By computing the Bogoliubov excitation, we further find that for both lattices Landau instability is present, which shows that the staggered state is not really a state at local energy minimum. For dynamical stability, we find that there exists a parameter region where the staggered state is free of dynamical instability for the checkerboard lattice whereas no such a parameter region is found for the square lattice. This suggests that the staggered state be of long life time in the former, but not the latter.

ACKNOWLEDGMENTS

The authors are grateful for very helpful discussions with A. Hemmerich. Y.X., Z.C., and B.W. are supported by the National Basic Research Program of MOST (NBRP) of China (2012CB921300, 2013CB921900), the National Natural Science Foundation (NSF) of China (10825417, 11274024), the Research Fund for the Doctoral Program of Higher Education (RFDP) of China (20110001110091). W.V.L is supported by the US DOD AFOSR (FA9550-12-1-0079), ARO (W911NF-11-1-0230), DARPA OLE Program through ARO, and the NSF of China (11128407). H.W. is supported by the NBRP of China (2011CB921503) and the NSF of China (11175246).

[1] Y. Tokura and N. Nagaosa, Science **288**, 462 (2000).
[2] I. Bloch, J. Dalibard, and W. Zwerger, Rev. Mod. Phys. **80**, 885 (2008).
[3] L. K. Lim, C. M. Smith, and A. Hemmerich, Phys. Rev. Lett. **100**, 130402 (2008).
[4] A. Isacsson and S. M. Girvin, Phys. Rev. A **72**, 053604 (2005).
[5] W. V. Liu and C. Wu, Phys. Rev. A **74**, 013607 (2006).
[6] A. B. Kuklov, Phys. Rev. Lett. **97**, 110405 (2006).
[7] A. Browaeys, H. Häffner, C. McKenzie, S. L. Rolston, K. Helmerson, and W. D. Phillips, Phys. Rev. A **72**, 053605 (2005).
[8] J. Sebby-Strabley, M. Anderlini, P. S. Jessen, and J. V. Porto, Phys. Rev. A **73**, 033605 (2006).
[9] M. Anderlini, J. Sebby-Strabley, J. Kruse, J. V. Porto, and W. D. Phillips, J. Phys. B **39**, S199 (2006).
[10] P. J. Lee, M. Anderlini, B. L. Brown, J. Sebby-Strabley, W. D. Phillips, and J. V. Porto, Phys. Rev. Lett. **99**, 020402 (2007).
[11] M. Anderlini, P. J. Lee, B. L. Brown, J. Sebby-Strabley, W. D. Phillips, and J. V. Porto, Nature (London) **448**, 452 (2007).
[12] T. Müller, S. Fölling, A. Widera, and I. Bloch, Phys. Rev. Lett **99**, 200405 (2007).
[13] G. Wirth, M. Ölschläger, and A. Hemmerich, Nature Phys. **7**, 147 (2011).
[14] M. Ölschläger, G. Wirth, and A. Hemmerich, Phys. Rev. Lett. **106**, 015302 (2011).
[15] M. Ölschläger, G. Wirth, T. Kock, and A. Hemmerich, Phys. Rev. Lett. **108**, 075302 (2012).
[16] P. Soltan-Panahi, D.-S. Lühmann, J. Struck, P. Windpassinger, and K. Sengstock, Nature Phys. **8**, 71 (2012).
[17] L. Tarruell, D. Greif, T. Uehlinger, G. Jotzu, and T. Esslinger, Nature (London) **483**, 302 (2012).
[18] A. Collin, J. Larson, and J.-P. Martikainen, Phys. Rev. A **81**, 023605 (2010).
[19] X. Li, E. Zhao, and W. V. Liu, Phys. Rev. A **83**, 063626 (2011).
[20] V. W. Scarola and S. Das Sarma, Phys. Rev. Lett **95**, 033003 (2005).
[21] C. Wu, W. V. Liu, J. Moore, and S. Das Sarma, Phys. Rev. Lett **97**, 190406 (2006).
[22] M. Lewenstein and W. V. Liu, Nature Phys. **7**, 101 (2011).
[23] Z. Cai and C. Wu, Phys. Rev. A **84**, 033635 (2011).
[24] B. Wu and Q. Niu, Phys. Rev. A **64**, 061603 (2001).
[25] Z. Chen and B. Wu, Phys. Rev. A **81**, 043611 (2010).
[26] H.-Y. Hui, R. Barnett, J. V. Porto, and S. Das Sarma, Phys. Rev. A **86**, 063636 (2012).
[27] L. Fallani, L. De Sarlo, J. E. Lye, M. Modugno, R. Saers, C. Fort, and M. Inguscio, Phys. Rev. Lett. **93**, 140406 (2004).
[28] J.-P. Martikainen, Phys. Rev. A **83**, 013610 (2011).
[29] V. M. Stojanović, C. Wu, W. V. Liu, and S. Das Sarma, Phys. Rev. Lett. **101**, 125301 (2008).
[30] M. Machholm, A. Nicolin, C. J. Pethick, and H. Smith, Phys. Rev. A **69**, 043604 (2004).